

The 2MASS Wide-Field T Dwarf Search. III. Seven New T Dwarfs and Other Cool Dwarf Discoveries

Adam J. Burgasser^{1,2,3}, Michael W. McElwain^{1,3}, J. Davy Kirkpatrick⁴, Kelle L. Cruz^{3,5},
Chris G. Tinney⁶, & I. Neill Reid^{3,7}

ABSTRACT

We present the discovery of seven new T dwarfs identified in the Two Micron All Sky Survey. Low-resolution ($R \sim 150$) 0.8–2.5 μm spectroscopy obtained with the IRTF SpeX instrument reveal the characteristic H_2O and CH_4 bands in the spectra of these brown dwarfs. Comparison to spectral standards observed with the same instrument enable us to derive classifications of T3 to T7 for the objects in this sample. Moderate-resolution ($R \sim 1200$) near-infrared spectroscopy for a subset of these discoveries reveal K I line strengths consistent with previously observed trends with spectral type. Follow-up imaging observations provide proper motion measurements for these sources, ranging from $< 0''.1$ to $1''.55 \text{ yr}^{-1}$. One object, 2MASS 0034+0523, has a spectrophotometric distance placing it within 10 pc of the Sun. This source also exhibits a depressed K-band peak reminiscent of the peculiar T dwarf 2MASS 0937+2931, and may be a metal-poor or old, high-mass brown dwarf. We also present low resolution SpeX data for a set of M and L-type dwarf, subdwarf, and giant comparison stars used to classify 59 additional candidates identified as background stars. These are primarily M5–M8.5 dwarfs, many exhibiting H I Paschen γ , but include three candidate ultracool M subdwarfs and one possible early-type L subdwarf.

Subject headings: stars: low mass, brown dwarfs — stars: fundamental parameters — stars: individual (2MASS J00345157+0523050, 2MASS J04070885+1514565, 2MASS J12095613–1004008, 2MASS J12314753+0847331, 2MASS J18283572–4849046, 2MASS J19010601+4718136, 2MASS J23312378–4718274) — stars: subdwarfs — techniques: spectroscopic

¹Department of Physics & Astronomy, University of California at Los Angeles, Los Angeles, CA, 90095-1562; adam@astro.ucla.edu, mcelwain@astro.ucla.edu

²Hubble Fellow

³Visiting Astronomer at the Infrared Telescope Facility, which is operated by the University of Hawaii under Cooperative Agreement NCC 5-538 with the National Aeronautics and Space Administration, Office of Space Science, Planetary Astronomy Program.

⁴Infrared Processing and Analysis Center, M/S 100-22, California Institute of Technology, Pasadena,

CA 91125; davy@ipac.caltech.edu

⁵Department of Physics & Astronomy, University of Pennsylvania, 209 South 33rd Street, Philadelphia, PA 19104; kelle@sas.upenn.edu

⁶Anglo-Australian Observatory, P.O. Box 296. Epping, NSW 1710, Australia; cgt@aoepp.aoa.gov.au

⁷Space Telescope Science Institute, 3700 San Martin Drive, Baltimore, MD 21218; inr@stsci.edu

1. Introduction

T dwarfs are a spectral class of brown dwarfs distinguished by the presence of CH₄, H₂O, and H₂ collision-induced absorption (CIA) in the near-infrared (Kirkpatrick et al. 1999; Burgasser et al. 2002; Geballe et al. 2002), and heavily pressure-broadened K I and Na I absorption at optical wavelengths (Tsuji, Ohnaka, & Aoki 1999; Burrows, Marley, & Sharp 2000; Burgasser et al. 2003c). These objects have effective temperatures (T_{eff}) ranging from \sim 1300 K at the transition between L and T dwarfs (Kirkpatrick et al. 2000; Stephens et al. 2001; Dahn et al. 2002; Vrba et al. 2004) to \sim 750 K for the latest-type T dwarf 2MASS 0415–0935 (Burgasser et al. 2002; Vrba et al. 2004). T dwarfs therefore comprise the coldest and intrinsically faintest brown dwarfs currently known, and as such are key objects for testing brown dwarf and extrasolar giant planet atmosphere models (Baraffe et al. 2003), probing the extreme low-mass end of the initial mass function (Allen et al. 2004; Burgasser 2004), and expanding the census of the Sun’s nearest neighbors.

For the past two years, we have been conducting a wide-field (74% of the sky) search for T dwarfs in the Two Micron All Sky Survey (Skrutskie et al. 1997; Cutri et al. 2003, hereafter 2MASS). This three-band, near-infrared (JHK_s) imaging survey samples the peak of the T dwarf spectral energy distribution, and is therefore the most sensitive wide-field sky survey currently available for identifying these cold brown dwarfs. Our results to date include the discovery of the bright, and therefore potentially very close ($d \approx 8$ pc) T dwarf 2MASS 1503+2525 (Burgasser et al. 2003d, hereafter Paper I) and three new T dwarfs identified in the Southern Hemisphere (Burgasser, McElwain, & Kirkpatrick 2003, hereafter Paper II). Here we

present the discovery of seven new T dwarfs in both Northern and Southern Hemispheres, all of which were verified by low resolution ($R \sim 150$) spectroscopic observations obtained with the IRTF 3.0m SpeX instrument (Rayner et al. 2003).

In § 2 we describe near-infrared imaging and spectroscopic observations of T dwarf candidates and comparison stars made using SpeX and other imaging instruments. In § 3 we analyze these data, classifying both the new T dwarfs and background stars, including four potential ultracool (spectral types later than sdM7) subdwarfs, using the low-resolution spectra and spectral comparison stars. We also report line strengths for the 1.243/1.252 μm K I doublet in six T dwarfs observed at moderate resolution ($R \sim 1200$) with SpeX, and proper motions for all of the T dwarf discoveries. In § 4 we discuss our results, including distance and tangential velocity estimates, signatures of gravity and/or metallicity in the near-infrared spectrum of 2MASS 0034+0523, and prospects for future discoveries. Results are summarized in § 5.

2. Observations

2.1. Target Selection

Our selection of T dwarf candidates from the 2MASS Working Point Source Database (WPSD) is described in detail in Paper I. In brief, we chose point sources with $J \leq 16$, $J - H \leq 0.3$ or $H - K_s \leq 0$, no optical counterpart with $5''$ in the USNO A2.0 catalog (Monet et al. 1998) or by visual inspection of Digitized Sky Survey (DSS) images, no catalogued minor planet counterpart, and $|b| \geq 15^\circ$. Revised 2MASS photometry for these sources is given in the All Sky Data Release (ADR) Point Source Catalog, and is based on improved photometric calibration, particularly at J -band (see Cutri et al. 2003, §IV.1.c). In some cases the new photome-

try pushes our candidates out of the initial selection criteria. However, these candidates were retained, and their ADR photometry is reported throughout this article. To date, a total of 912 T dwarf candidates have been observed as part of this search program.

2.2. Imaging

Follow-up near-infrared imaging observations of T dwarf candidates are required to eliminate the majority of contaminant sources. These include minor planets whose ephemerides were unknown or were not incorporated at the time of 2MASS data processing, and image artifacts that remain in the 2MASS WPSD. Imaging observations also provide second epoch astrometry for confirmed T dwarfs that may be used to measure proper motion. We therefore conducted a series of imaging campaigns using various instrumentation on 1-4m class telescopes.

2.2.1. IRTF 3.0m SpeX

The SpeX instrument is comprised of a 1024×1024 InSb array as the primary detector for the spectrograph, and a second 512×512 InSb array imaging/guiding camera with a $60'' \times 60''$ field-of-view ($0''.12$ pixels). We made use of the latter detector to image T dwarf candidates during our 2003 September 17–19 (UT) IRTF observing campaign. Conditions varied from clear to slightly hazy with seeing between $0''.5$ – $0''.7$ at J -band. Dithered exposure pairs of 30 s each were obtained at J -band and pair-wise subtracted for inspection. We verified that each exposure was at least as deep as the corresponding 2MASS image.

Table 1 lists those sources that were absent in follow-up images. Five of these were identified as known asteroids using the Small-Body Search Tool maintained by the Jet Propulsion Laboratory Solar System Dynamics Group¹,

and were typically catalogued as asteroids after the 2MASS observation. The remaining sources have ecliptic latitudes $|\beta| < 15^\circ$ and are therefore also likely to be as yet uncatalogued minor planets.

2.2.2. Palomar 1.5m CCD Camera

Gunn- z band images of four new T dwarfs identified in this sample (see § 3.1.2) were obtained using the Palomar 1.5m facility CCD Camera on 2003 September 27 (UT). Conditions were clear and photometric with $0''.7$ seeing. The CCD camera is a red-sensitive, 2048×2048 , thinned detector with $24\mu\text{m}$ pixels. Pixel scale on the sky is $0''.378$. Only the central 1024×1024 region was used for a total field of view of $6''.5$ on a side. Raw images were bias-subtracted and divided by a median-combined flat field frame generated from a series of lamp on/off exposures reflected from the interior dome. All four T dwarf targets were detected in these images to sufficient signal-to-noise ($\text{S/N} \gtrsim 10$) to obtain reliable astrometry.

2.2.3. Lick 3.0m Gemini

The Lick 3.0m Gemini instrument (McLean et al. 1993) is a dual 256×256 HgCdTe/InSb camera with $0''.68$ pixels and a $3' \times 3'$ field of view. J-band images of 2MASS 1209–1004 were obtained using this instrument on 2003 May 12 (UT); conditions were clear with seeing of $1''.2$. Observations were similar to those described in Paper I, with a dithered pair of 30 s exposures obtained and differenced to produce the final science image; no additional calibration was required for the astrometric measurements.

2.2.4. AAT 3.9m IRIS2

The AAT 3.9m IRIS2 near-infrared imager and spectrograph² is a 1024×1024 HgCdTe

¹See http://ssd.jpl.nasa.gov/cgi-bin/sb_search.

²See <http://www.aoa.gov.au/iris2/index.html>.

array camera with $0''.4486$ pixels and a $7''.7 \times 7''.7$ field of view. We used this camera to observe 2MASS 1231+0847, 2MASS 1828–4849, and 2MASS 2331–4718 on 2003 June 11 and 2003 September 10 and 13 (UT). These data are part of an imaging program testing the use of CH₄ filters to efficiently identify and classify T dwarf candidates; the program is described in detail in Tinney et al. (in preparation). Conditions during the observations were non-photometric, with occasional cloud patches, although data were only obtained when the sky was clear. Seeing ranged from $0''.9$ – $2''.0$. Targets were observed in dithered sets of three 40 s exposures in each of the CH₄-s and CH₄-l filters, which bisect the *H*-band about the 1.6 μm CH₄ band. Images were processed via the IRIS2 data reduction pipeline, which is modeled after the UKIRT ORAC-DR pipeline³, and includes bad pixel masking, flat fielding, and alignment and re-sampling of the dithered exposures to produce a final, calibrated image.

2.3. Spectroscopy

A total of 66 T dwarf candidates and 33 spectral comparison stars were observed using the low-resolution prism mode of the SpeX spectrograph primarily over two observing runs, 21–23 May 2003 and 17–19 September 2003 (UT). A log of observations for the candidates and comparison stars are given in Tables 2 and 3, respectively. Conditions during the May run ranged from light to heavy cirrus with seeing of $0''.5$ – $0''.9$ at *J*-band. One object, 2MASS 0034+0523, was observed on 5 September 2003 (UT) during clear conditions with similar seeing. The prism mode of SpeX provides 0.7–2.5 μm continuous spectroscopy in a single order. Using the $0''.5$ slit, we obtained a resolution $R \sim 150$; dispersion on the chip is 20 – 30 \AA pixel^{−1}. For all observations, the instrument rotator was positioned at the

parallactic angle to mitigate differential color refraction across the broad spectral band observed. Total integration times ranged from 12 (bright M giant and supergiant stars) to 1600 s, and were typically obtained in multiple pairs of 180 s exposures dithered along the chip for sky subtraction. Except for a few low declination sources, the majority of objects were observed at airmasses $\lesssim 1.5$. In all but one case, we observed A0 stars selected from the Henry Draper (HD) catalog shortly before or after the target observation and at a differential airmass $\lesssim 0.1$ for flux calibration. Internal flat-field and Ar arc lamps were observed immediately after the A0 star observations for instrumental calibration.

Six T dwarfs, including five of the discoveries presented here, were also observed using the cross-dispersed, moderate-resolution SXD mode of SpeX during the May and September runs. These observations are summarized in Table 4. We employed the same $0''.5$ slit as the prism observations to obtain $R \sim 1200$ spectra from 0.9–2.4 μm in four orders; an additional order subtending 0.81–0.95 μm was measured for the bright T5.5 2MASS 1503+2525. Pixel dispersion on the chip ranged from 2.7 to 5.3 \AA pixel^{−1}. We observed all targets with the slit rotated to the parallactic angle in dithered pairs of 300 s each, with total integration times of 1800–3000 s. A0V/A0Vn HD stars and internal calibration lamps were observed immediately after each target observation.

All data were reduced using the Spextool package (Cushing, Vacca, & Rayner 2004). For both the prism and SXD datasets, science data were corrected for linearity, pairwise subtracted, and divided by the corresponding median-combined flat field image. Spectral data were optimally extracted using the default settings for aperture and background source regions, and wavelength calibration was determined from arc lamp and sky emission lines. Multiple spectral obser-

³See <http://www.jach.hawaii.edu/JACpublic/UKIRT/software/oracdr/index.html>.

vations for each source were then median-combined after scaling the spectra to match the highest signal-to-noise observation. Telluric and instrumental response corrections for the science data were determined using the method outlined in Vacca et al. (2003). For the prism observations, line shape kernels were derived from the arc lines; for the SXD observations, they were derived from the 1.005 μm H I Paschen δ line in the A0 calibrator spectra. Adjustments were made to the telluric spectra to compensate for differing H I line strengths and velocity shifts. Final calibration was made by multiplying the observed target spectrum by its respective telluric correction spectrum. For the SXD data, multiple orders for each target exposure were scaled and combined using the corresponding low-resolution prism spectrum as a relative flux template.

3. Analysis

3.1. Low Resolution Spectroscopy

3.1.1. Background Stars

Examination of the low-resolution spectra indicate that the majority of these candidate sources are late-type M dwarfs, based on the presence of weak H_2O absorption at 1.4 and 1.9 μm ; CO absorption at 2.3 μm ; TiO and VO bands at 0.7–1.0 μm ; and FeH, Na I, and K I absorption at *J*-band. This result is not unexpected, as many of these sources have $J \sim 16$, implying $R - J \gtrsim 3-5$ at the detection limit of the DSS plates (Reid 1991), typical for late-type M dwarfs (Kirkpatrick et al. 1999). The faintness of these objects also imply significant errors in their 2MASS photometry, which explains in part their unusually blue $J - K_s$ colors.

Nevertheless, to better understand the nature of these contaminant sources, we classified their spectra by comparison to a suite of M- and L-type spectral standards and known

objects, as listed in Table 3. A representative sample of these comparison spectra are shown in Figure 1. For the dwarfs, the strengthening of the 1.4 and 1.9 μm H_2O bands, and 0.99 and 1.2 μm FeH bands; appearance of the 1.17 and 1.25 μm K I doublets; weakening of the 0.76, 0.82, and 0.84 μm TiO bands; shift in peak flux toward 1.3 μm ; and reddening of the 1.3–2.4 μm spectral energy distribution are all correlated with spectral type. Subdwarfs show distinctively stronger 0.99 μm FeH absorption and weaker CO and TiO absorption than the dwarfs for equivalent H_2O band strengths, as well as a shift in the peak of their spectral energy distributions to shorter wavelengths. Giant and supergiant M stars exhibit much deeper H_2O bands and stronger VO, TiO, and CO absorption, but fairly weak or absent metal hydride bands and atomic lines.

Using these diagnostics and the comparison spectra, we visually classified each of the observed sources that were not identified as T dwarfs. These classifications, which we estimate are accurate to within ~ 0.5 –1.0 subtypes, are listed in Table 2; uncertain numerical or luminosity classifications due to low S/N data are noted by a colon. A large percentage of the late-type M dwarfs exhibit H I Paschen γ emission (1.09 μm): 33% (6 of 18) of the M7–M7.5 dwarfs and 66% (12 of 18) of the M8–M8.5 dwarfs appear to be in emission, but none of the M5–M6.5 dwarfs. The observed emission is consistent with the high frequency ($\sim 100\%$) of $\text{H}\alpha$ emission seen in the optical spectra of M7–M8 dwarfs (Gizis et al. 2000).

While most of the background sources exhibit spectral energy distributions and absorption features similar to the dwarf comparison stars, a handful of sources appear to be peculiar. These include four objects that exhibit subdwarf characteristics. As shown in Figure 2, 2MASS 0142+0523, 2MASS 1640+1231, and 2MASS 1640+2922 all ap-

pear to be similar to or somewhat later than the sdM7.5 LSR 2036+5059 (Lepine, Rich, & Shara 2003a), with strong 0.86, 0.99, and 1.2 μm FeH absorption; weak 2.3 μm CO absorption; moderately strong 1.4 and 1.9 μm H₂O absorption; and a relatively blue 1–2.5 μm spectral slope. Another source, 2MASS 0041+3547, exhibits spectral features similar to the L1 standard 2MASS 1439+1929 (Kirkpatrick et al. 1999), but has stronger 0.86 and 0.99 μm FeH absorption, weaker CO, and a somewhat bluer 1.3–2.4 μm spectral slope. This object may be a new early-type L subdwarf, similar to LSR 1610-0040 (Lepine, Rich, & Shara 2003b). However, as there currently exists no classification scheme for ultracool subdwarfs at near-infrared wavelengths, we characterize these sources as candidate subdwarfs for the time being; further spectral analysis will be presented in a future publication. It should be noted that only four subdwarfs later than type M7 are currently known (Burgasser et al. 2003b; Lepine, Rich, & Shara 2003a,b; Lepine, Shara, & Rich 2003).

Finally, we address one additional background source, 2MASS 1733+1529, classified here as a DC 10 white dwarf based on its blackbody slope and absence of H I absorption lines (Figure 3). This object was selected because of its absence in the first generation Palomar Sky Survey (POSS-I) *R*-band plate (Figure 4, left), although it is present on the *B*-band plate as well as the *B*-, *R*- (Figure 4, right), and *I*-band plates of POSS-II. The absence of this source in the POSS-I *R*-band image was independently verified by M. Gray and R. Humphreys to a faint limit of $R \sim 19.5$ –20.0 using the Minnesota Automated Plate Scanner Catalog⁴, and by visual examination of POSS-I prints available at the Caltech Astrophysics Library. 2MASS 1733+1529 is not listed in the McCook &

Sion (1999) white dwarf catalog; and its small proper motion, $0\rlap{.}^{\prime\prime}05 \pm 0\rlap{.}^{\prime\prime}04 \text{ yr}^{-1}$, measured from Lick 3m Gemini *J*-band imaging (see § 3.3), excludes it from the NLTT (Luyten 1979) and revised NLTT (Salim & Gould 2003) proper motion catalogs. As this source is relatively bright in the optical ($R = 16.9$ in the USNO-B1.0 Catalog; Monet et al. 2003), and given the absence of any obvious photographic anomaly, it is unclear as to why it was undetected on the POSS-I *R*-band plate. It is possible that 2MASS 1733+1529 was obscured in this image by an eclipsing or transiting faint source, such as a low-mass stellar or substellar companion. Monitoring observations are planned to verify or place stringent constraints on this intriguing hypothesis.

3.1.2. *T* Dwarf Discoveries

Seven of the candidates listed in Table 2 exhibit clear absorption features of H₂O (1.1, 1.4, and 1.9 μm) and CH₄ (1.3, 1.6, and 2.2 μm) in their low-resolution spectra, characteristic of *T* dwarfs. Finder charts for these objects are given in Figure 5, low-resolution spectra are diagrammed in Figure 6, and spectrophotometric properties are listed in Table 5. These objects exhibit a broad range of CH₄ band strengths and near-infrared colors ($-0.7 < J - K_s < 0.85$), encompassing early-, mid-, and late-type *T* dwarf spectral morphologies (Burgasser et al. 2002; Geballe et al. 2002).

The new *T* dwarfs were classified by their low-resolution spectra following the technique of Burgasser et al. (2002), which is based on the established MK Process of spectral classification (e.g., Morgan 1984). In addition to our candidates, we observed a set of five *T* dwarf spectral standards: SDSS 0423–0414 (T0), SDSS 1254–0122 (T2), 2MASS 2254+3123 (T4), 2MASS 0243–2453 (T6), and 2MASS 0415–0935 (T8). The T2, T6, and T8 standards are those established

⁴MAPS; see <http://aps.umn.edu/index.html>.

in Burgasser et al. (2002), while the T0 and T4 standards were selected as part of an expanded list of spectral standards given in Burgasser et al. (2003a). To quantify our classifications, we used revised spectral indices from the latter reference which sample the major H₂O and CH₄ bands in the 1–2.5 μm region while avoiding strong telluric absorption regions. These indices are defined as:

$$H_2O^J = \frac{\int F_{1.14-1.165}}{\int F_{1.26-1.285}}, \quad (1)$$

$$CH_4^J = \frac{\int F_{1.30-1.325}}{\int F_{1.26-1.285}}, \quad (2)$$

$$H_2O^H = \frac{\int F_{1.48-1.52}}{\int F_{1.56-1.60}}, \quad (3)$$

$$CH_4^H = \frac{\int F_{1.635-1.675}}{\int F_{1.56-1.60}}, \quad (4)$$

and

$$CH_4^K = \frac{\int F_{2.215-2.255}}{\int F_{2.08-2.12}}, \quad (5)$$

where $\int F_{\lambda_1-\lambda_2}$ designates the integrated flux between wavelengths λ_1 and λ_2 , and indices are defined as the ratio of flux at the base of the absorption band to the nearby pseudo-continuum⁵. These spectral indices were measured for all T dwarfs in our low-resolution spectral sample. Classifications for each index (excluding the spectral standards) were determined as the closest match to the standard values, allowing for subtypes halfway between the standard classes (i.e., integer subclasses). Final classifications for each object were determined as the mean of the individual index classifications, rounded off to the nearest 0.5 subclass.

Table 6 lists the spectral indices and derived classifications for the new and previously

⁵The presence of overlying opacity throughout the 1–2.5 μm region implies that no true continuum is present; we therefore normalize to the local spectral maximum, or pseudo-continuum.

known T dwarfs. The scatter amongst individual index subtypes is typically 0.4–0.7 subclasses, with some objects exhibiting no scatter, justifying our 0.5 subclass precision. As a check, we compared derived subtypes to those from the literature for seven previously identified and classified T dwarfs; all were consistent within 0.5 subclasses. We also examined the behavior of the indices with spectral type, as shown in Figure 7; all five indices show minimal scatter about a line connecting the standard values, again consistent with the adopted classification precision. The scatter in these indices is in fact better than that seen in the classifications of Burgasser et al. (2002) and Geballe et al. (2002), reflecting overall higher signal-to-noise data and the improved spectral index definitions. The spectral types for the T dwarf discoveries range from T3 (2MASS 1209–1004) to T7 (2MASS 0034+0523), the former object being the earliest-type T dwarf so far identified in our 2MASS search. As shown in Figure 6, the derived classifications are consistent with a monotonic increase in H₂O and CH₄ bandstrengths with spectral type.

3.2. Moderate Resolution Spectroscopy

Moderate resolution SpeX spectra of six T dwarfs are shown in Figure 8. These data reveal the complex H₂O and CH₄ molecular features in far greater detail than the prism spectra. While the S/N of the higher resolution spectra are on average lower (10–50%), most of the structure seen is real and repeats between the objects. These data also resolve the 1.243/1.252 μm K I doublet, shown in detail in Figure 8, a key diagnostic of temperature at the brightest peak in the spectral energy distribution. Pseudo-equivalent widths (PEWs; equivalent width relative to the pseudo-continuum) for these lines were measured following the method outlined in Paper II, directly integrating over

the line profiles. Results are given in Table 7. The strongest lines are found in the T5 2MASS 2331–4718, which have PEWs of 8.5 ± 0.7 and 12.8 ± 0.6 Å for the 1.243 and 1.252 μm K I lines, respectively. Indeed, with the exception of the T5.5 2MASS 0516–0445 (for which only low S/N data have been obtained), these are the strongest K I lines measured in any T dwarf to date (Burgasser et al. 2002; Burgasser, McElwain, & Kirkpatrick 2003; McLean et al. 2003). Both 2MASS 1503+2525 and 2MASS 1231+0847 exhibit broadened K I lines, possibly due to rapid rotation or high photospheric pressure, the latter case indicative of high surface gravity. Also note the nearly absent K I lines in the T7 2MASS 0034+0523, due either to its low T_{eff} or possibly metal deficiency (see § 4.2). Overall, the observed line strengths are in general agreement with previous work, with the strongest K I lines found amongst the T5 dwarfs and becoming progressively weaker toward the later spectral types.

3.3. Astrometry

Proper motions for the T dwarf discoveries were measured using 2MASS ADR data and the follow-up imaging observations described in § 2.2. Data analysis was similar to that described in Paper II. We used 2MASS catalog data as first epoch astrometry, while the follow-up images, taken roughly 3–5 years after the 2MASS observations, comprised our second epoch dataset. 2MASS sources within the re-imaged areas (excluding the T dwarf) were matched to detected sources on the follow-up images. First-order coordinate solutions for the images were then determined by linear regression using this grid of background stars, allowing for the rejection of 3σ outliers (i.e., moving sources). For the IRIS2 (CH₄-s images only) and CCD observations, ~ 15 –60 background sources were used, yielding positional uncertainties of $0''.1$ –

$0''.4$, equivalent to 2MASS astrometric accuracy (Cutri et al. 2003), and proper motion uncertainties of $\lesssim 0''.1 \text{ yr}^{-1}$. For the Gemini observation of 2MASS 1209–1004, only four background objects were available and astrometric uncertainties were assumed to be somewhat higher. Using these coordinate solutions, the second epoch position of the T dwarf was computed and its motion derived. We note that the agreement between proper motion determinations for 2MASS 0034+0523 obtained with the Palomar 60" CCD Camera and AAT IRIS2 lend confidence to the reliability of our measurements.

Table 8 lists the resulting proper motions. As expected for a nearby population of faint brown dwarfs, these objects have large motions in general, with 2MASS 1231+0847 exhibiting the largest at $1''.55 \pm 0''.07 \text{ yr}^{-1}$. This object would be easily identified in a near-infrared proper motion survey. On the other hand, two T dwarfs, 2MASS 0407+1514 and 2MASS 2331–4718, have motions below our sensitivity limits. We discuss the associated tangential velocities for these T dwarfs below.

4. Discussion

4.1. Spectrophotometric Distances

Using the derived classifications and 2MASS photometry, it is possible to estimate the spectrophotometric distances of our T dwarf discoveries. We employed the polynomial J - and K_s -band absolute magnitude/spectral type relations from Tinney, Burgasser, & Kirkpatrick (2003), based on parallax measurements from their own program and from Dahn et al. (2002). Distance estimates for each of the newly discovered T dwarfs were calculated in both bands (with the exception of 2MASS 0034+0523 which was not detected at K_s by 2MASS) and for ± 0.5 subclasses about the nominal classification. Final distances and uncertainties were determined by the mean

and standard deviation of these estimates, respectively, and are listed in Table 5. Assuming that they are single sources, all of the objects listed are within 25 pc of the Sun, with the most distant object being the earliest-type T dwarf 2MASS 1209–1004. Three objects, 2MASS 0034+0523, 2MASS 1231+0847, and 2MASS 1828–4849, are at or within 10 pc from the Sun within the reported uncertainties, with the first (and latest-type) object having an estimated distance of only 8.2 ± 1.5 pc. It should be noted that the uncertainties in these distance estimates do not take into account systematic deviations in the absolute magnitude/spectral type relation (Tinney, Burgasser, & Kirkpatrick 2003) nor possible duplicity, and should be confirmed by parallax measurement.

Combining the distance estimates with the proper motion determinations from § 3.3, we calculated tangential velocities for these T dwarfs, listed in Table 8. The mean V_{tan} of those T dwarfs with detected motion is 43 km s^{-1} with a standard deviation of 28 km s^{-1} ; including the upper limits yields a somewhat lower mean of 33 km s^{-1} . This value is consistent with the mean V_{tan} for disk dwarfs (39 km s^{-1} ; Reid & Hawley 2000) but is somewhat higher than that for field late-type M and L dwarfs (22 km s^{-1} ; Gizis et al. 2000), suggesting that the T dwarfs in this sample may be drawn from a somewhat older population. A similar difference in the V_{tan} distribution between field L and T dwarfs has also been noted by Vrba et al. (2004), and a mean age difference between these classes is predicted in field substellar mass function simulations (Burgasser 2004). This possible age segregation is consistent with the evolution of brown dwarfs, as an object of a given mass will evolve from warm (L dwarf) to cold (T dwarf) as it ages; however, a larger sample must be considered before drawing any firm conclusions about the relative ages of the L and T dwarf

field populations.

We note that the spectrophotometric distance of 2MASS 1231+0847 is consistent within its uncertainties to the nearby (13.4 ± 0.3 pc; HIPPARCOS; Perryman et al. 1997) K7V star Gliese 471, located roughly 8.1 (6500 AU) to the northwest. Indeed, 2MASS 1231+0847 was also identified in a parallel search for wide brown dwarf companions to nearby stars currently being conducted by J. D. Kirkpatrick. However, while their direction of motion is nearly identical ($\sim 230^\circ$), 2MASS 1231+0847 has a proper motion nearly twice as large as Gliese 471, and is therefore not a bound companion.

4.2. Gravity/Metallicity Signatures at K-band

The T7 2MASS 0034+0523 has the bluest $J - K_s$ color amongst the T dwarf discoveries, and it may be even bluer as 2MASS photometry provides only an upper limit. Examination of near-infrared spectral data confirms this color, as 2MASS 0034+0523 exhibits a fairly suppressed K -band peak in comparison to the rest of the T6–T8 dwarfs observed. This is quantified in Figure 9, which plots the logarithm of the spectral ratio

$$K/J = \frac{\int F_{2.06-2.10}}{\int F_{1.25-1.29}} \quad (6)$$

as a function of spectral type for all of the T dwarfs observed. SpeX prism data are ideally suited for this measurement, as the full near-infrared spectral range is sampled in a single order and no correction is required to match the relative scalings between the J - and K -bands. The ratio exhibits a tight linear trend across the full spectral type range of T dwarfs, although there is a somewhat greater spread in values amongst the T5–T6 dwarfs. 2MASS 0034+0523 stands well above this trend, however, having the smallest value of K/J , and

hence the most suppressed K -band peak, in the entire sample.

The spectral properties of this source are reminiscent of the peculiar T6 2MASS 0937+2931 (Burgasser et al. 2002), which not only has a very blue near-infrared color ($J - K_s = -0.62 \pm 0.14$; Paper I), likely due to enhanced CIA H_2 absorption, but also strong absorption from the pressure-broadened $0.77 \mu\text{m}$ K I resonance doublet and the $0.99 \mu\text{m}$ FeH band (Burgasser et al. 2003c). The enhanced pressure-sensitive features are symptomatic of a high pressure photosphere, which can exist on a brown dwarf with a high surface gravity (i.e., old and massive) and/or a metal deficient atmosphere (Burrows et al. 2002). Indeed, strong FeH and CIA H_2 absorption are hallmarks of cool halo subdwarf spectra (Figure 1), which are themselves typically older and metal-poor, and 2MASS 0937+2931 has been interpreted as a possible thick disk or halo brown dwarf (Burrows et al. 2002; Burgasser et al. 2003c). 2MASS 0034+0523, like 2MASS 0937+2931, also has exceedingly weak $1.243/1.252 \mu\text{m}$ K I lines that may be due to reduced metallicity or higher surface gravity (Burrows et al. 2002), although its late spectral type (and hence cool temperature) may be the dominant factor. 2MASS 0034+0523 does not have a large V_{tan} as might be expected for a halo star, although on an individual basis this does not rule out its membership in an older kinematic population. Clearly, a more detailed study of both of these peculiar T dwarfs is needed to assess metallicity and/or gravity effects in cool brown dwarf spectra.

4.3. Prospects for Further Discoveries

To date, we have observed roughly 70% of our 2MASS search sample, identifying 31 T dwarfs, 8 of which have estimated or measured (Dahn et al. 2002; Tinney, Burgasser, & Kirkpatrick 2003; Vrba et al. 2004) distances

within 10 pc of the Sun. This is roughly consistent with the predicted numbers from Paper I ($\sim 35\text{--}45$ T dwarfs), although we have uncovered less than half of the ~ 20 T dwarfs predicted to have distances less than 10 pc. Many of the latter are probably late-type T dwarfs, $T_{eff} \lesssim 1000 \text{ K}$, too faint to be detected by 2MASS beyond a few parsecs. In addition to these very low-luminosity sources, our search has identified one *bona-fide* ultracool halo subdwarf, the late-type sdL 2MASS 0532+8246 (Burgasser et al. 2003b), and now four candidate late-type subdwarfs requiring further verification. In retrospect, the search criteria employed are well-suited for identifying these metal-deficient objects, which have red optical/near-infrared colors, peak in flux at J -band, and exhibit relatively blue $J - K_s$ colors due to enhanced CIA H_2 absorption (Leggett et al. 2000). Such serendipitous discoveries provide a new opportunity for exploring the physical properties, particularly metallicity and age diagnostics, of very cool stars and brown dwarfs.

5. Summary

We have discovered seven new T dwarfs in the 2MASS survey with spectral types ranging from T3 to T7, spectrophotometric distances of 8.2 to 23 pc, and proper motions from our detection limit ($0.^{\circ}1 \text{ yr}^{-1}$) to $1.^{\circ}55 \text{ yr}^{-1}$. This sample adds substantially to the current census of T dwarfs, now around 50 objects. We have also identified four candidate ultracool subdwarfs, including one possible early-type L subdwarf, which share the blue near-infrared colors and red optical/near-infrared colors of our T dwarf discoveries. We estimate that several T dwarfs remain to be identified in our sample, and possibly many more cool subdwarfs, yielding new targets in our quest to understand the observational properties of the lowest-mass stars and brown dwarfs in the Solar Neighborhood.

We thank our telescope operators Bill Golisch, Dave Griep, and Paul Sears, and instrument specialist John Rayner, for their support during the IRTF observations, and the IRTF TAC for its generous allocation of time for this project. We also thank Matt Gray and Roberta Humphreys at the University of Minnesota, Jean Mueller at Palomar Observatory, and the library staff at the Caltech Astrophysics Library, for their assistance in obtaining, examining, and verifying POSS-I images of 2MASS 1733+1529. We are grateful to our referee for her/his prompt and thorough review of the original manuscript. A. J. B. acknowledges support provided by NASA through Hubble Fellowship grant HST-HF-01137.01 awarded by the Space Telescope Science Institute, which is operated by the Association of Universities for Research in Astronomy, Incorporated, under NASA contract NAS5-26555. K. L. C. acknowledges support from a NSF Graduate Research Fellowship. This research has made use of the SIMBAD database, operated at CDS, Strasbourg, France. POSS-I, POSS-II, SERC, and AAO *R*-band images were obtained from the Digitized Sky Survey image server maintained by the Canadian Astronomy Data Centre, which is operated by the Herzberg Institute of Astrophysics, National Research Council of Canada. The Digitized Sky Survey was produced at the Space Telescope Science Institute under U.S. Government grant NAG W-2166. The images of these surveys are based on photographic data obtained using the Oschin Schmidt Telescope on Palomar Mountain and the UK Schmidt Telescope. The plates were processed into the present compressed digital form with the permission of these institutions. This publication makes use of data from the Two Micron All Sky Survey, which is a joint project of the University of Massachusetts and the Infrared Processing and Analysis Center, funded by the National

Aeronautics and Space Administration and the National Science Foundation. 2MASS data were obtained from the NASA/IPAC Infrared Science Archive, which is operated by the Jet Propulsion Laboratory, California Institute of Technology, under contract with the National Aeronautics and Space Administration. The authors wish to extend special thanks to those of Hawaiian ancestry on whose sacred mountain we are privileged to be guests. Electronic copies of the spectra presented here can be obtained directly from the primary author.

REFERENCES

Allen, P. R., et al. 2004, ApJ, in preparation

Baraffe, I., Chabrier, G., Barman, T., Allard, F., & Hauschildt, P. H. 2003, A&A, 402, 701

Burgasser, A. J. 2004, ApJ, in preparation

Burgasser, A. J., Golimowski, D. A., Geballe, T. R., Leggett, S. K., & Kirkpatrick, J. D. 2003a, in IAU Symposium 211: Brown Dwarfs, ed. E. L. Martin (San Francisco: ASP), p. 377

Burgasser, A. J., Kirkpatrick, J. D., Burrows, A., Liebert, J., Reid, I. N., Gizis, J. E., McGovern, M. R., Prato, L., & McLean, I. S. 2003b, ApJ, 592, 1186

Burgasser, A. J., Kirkpatrick, J. D., Liebert, J., & Burrows, A. 2003c, ApJ, 594, 510

Burgasser, A. J., Kirkpatrick, J. D., McElwain, M. W., Cutri, R. M., Burgasser, A. J., & Skrutskie, M. F. 2003d, AJ, 125, 850 (Paper I)

Burgasser, A. J., Kirkpatrick, J. D., Reid, I. N., Brown, M. E., Miskey, C. L., & Gizis, J. E. 2003e, ApJ, 586, 512

Burgasser, A. J., McElwain, M. W., & Kirkpatrick, J. D. 2003, AJ, 126, 2487 (Paper II)

Burgasser, A. J., et al. 1999, ApJ, 522, L65

—. 2000, ApJ, 531, L57

—. 2002, ApJ, 564, 421

Burrows, A., Burgasser, A. J., Kirkpatrick, J. D., Liebert, J., Milsom, J. A., Sudarsky, D., & Hubeny, I. 2002, ApJ, 573, 394

Burrows, A., Marley, M. S., & Sharp, C. M. 2000, ApJ, 531, 438

Cruz, K. L., Reid, I. N., Liebert, J., Kirkpatrick, J. D., & Lowrance, P. J. 2003, AJ, 126, 242

Cushing, M. C., Vacca, W. D., & Rayner, J. T. 2004, PASP, in press

Cutri, R. M., et al. 2003, Explanatory Supplement to the 2MASS All Sky Data Release, <http://www.ipac.caltech.edu/2mass/releases/allsky/doc/expsup.html> (2003, ApJS, 125, 184) (USNO-B1.0 Catalog)

Dahn, C. C., et al. 2002, AJ, 124, 1170

Geballe, T. R., et al. 2002, ApJ, 564, 466

Gizis, J. E. 2002, ApJ, 575, 484

Gizis, J. E., Monet, D. G., Reid, I. N., Kirkpatrick, J. D., Liebert, J., & Williams, R. 2000, AJ, 120, 1085

Hawley, S. L. et al. 2002, AJ, 123, 3409

Kirkpatrick, J. D., Henry, T. J., & McCarthy, D. W., Jr. 1991, ApJS, 77, 417

Kirkpatrick, J. D., Reid, I. N., Liebert, J., Gizis, J. E., Burgasser, A. J., Monet, D. G., Dahn, C. C., Nelson, B., & Williams, R. J. 2000, AJ, 120, 447

Kirkpatrick, J. D., et al. 1999, ApJ, 519, 802

Leggett, S. K., et al. 2000, ApJ, 536, L35

Lepine, S. Rich, R. M., & Shara, M. M. 2003a, AJ, 125, 1598

—. 2003b, ApJ, 591, L49

Lepine, S. Shara, M. M., & Rich, R. M. 2002, AJ, 124, 1190

—. 2003, ApJ, 585, L69

Luyten, W. J. 1979, New Luyten Catalogue of Stars with Proper Motions Larger than Two Tents of an Arcsecond (NLTT Catalog) (Minneapolis: Univ. Minn. Press)

McCook, G. P., & Sion, E. M. 1999, ApJS, 121, 1

McLean, I. S., McGovern, M., Burgasser, A. J., Prato, L., Kirkpatrick, J. D., & Kim, S. S. 2003, ApJ, 596, 561

McLean, I. S., et al. 1993, SPIE, 1946, 513

Monet, D. G., et al. 1998, USNO-A2.0 Catalog (Flagstaff: USNO)

Morgan, W. W. 1984, in The MK Process and Stellar Classification, Proceedings of the Workshop in honour of W. W. Morgan and P. C. Keenan, ed. R. F. Garrison (Toronto: David Dunlap Observatory), p.18

Rayner, J. T., Toomey, D. W., Onaka, P. M., Denault, A. J., Stahlberger, W. E., Vacca, W. D., Cushing, M. C., & Wang, S. 2003, PASP, 115, 362

Reid, I. N. 1991, AJ, 102, 1428

Reid, I. N., & Hawley, S. L. 2000, New Light on Dark Stars (Chichester: Praxis)

Salim, S., & Gould, A. 2003, ApJ, 582, 1011 (Revised NLTT Catalog)

Skrutskie, M. F., et al. 1997, in The Impact of Large-Scale Near-IR Sky Surveys, ed. F. Garzon (Dordrecht: Kluwer), p. 25

Stephens, D. C., Marley, M. S., Noll, K. S., &
Chanover, N. 2001, ApJ, 556, L97

Strauss, M. A., et al. 1999, ApJ, 522, L61

Tinney, C. G., Burgasser, A. J., & Kirkpatrick, J. D. 2003, AJ, 126, 975

Tsuiji, T., Ohnaka, K., & Aoki, W. 1999, ApJ, 520, L119

Vacca, W. D., Cushing, M. C., & Rayner, J. T. 2003, PASP, 155, 389

Vrba, F. J., et al. 2004, AJ, submitted

TABLE 1
T DWARF CANDIDATES ABSENT IN FOLLOW-UP SPEX IMAGING.

Object ^a (1)	β (°) (2)	2MASS Observations ^b					Identification ^c (7)
		UT Date (3)	<i>J</i> (4)	<i>J</i> − <i>H</i> (5)	<i>H</i> − <i>K_s</i> (6)		
2MASS J00344717−3343404	−34	1998 Oct 3	15.77±0.05	0.40±0.10	−0.17±0.22	1999 XJ197	
2MASS J02132776+1939028	6	1997 Oct 19	15.87±0.06	0.30±0.13	0.18±0.19		
2MASS J02273983+1824524	4	1997 Oct 20	15.25±0.05	0.52±0.07	−0.10±0.12	2001 TL10	
2MASS J02322515+2942172	14	1997 Nov 10	14.61±0.04	0.30±0.05	0.18±0.06		
2MASS J02381005+2725209	11	1997 Nov 10	15.56±0.05	0.36±0.09	−0.11±0.15		
2MASS J02470189+2200236	6	1997 Oct 15	15.73±0.07	0.15±0.15	0.41±0.22		
2MASS J03153063+2101434	3	2000 Nov 8	15.87±0.09	0.10±0.18	−0.07±0.27		
2MASS J03483407+3231433	12	1998 Jan 25	15.54±0.05	0.35±0.10	−0.01±0.15	2002 AW2	
2MASS J04122822+1316535	−8	2000 Nov 26	15.96±0.07	0.64±0.12	0.00±0.17	2000 UA110	
2MASS J04185615+2527216	4	1997 Nov 29	15.96±0.06	0.33±0.11	−0.01±0.19		
2MASS J04265381+1158063	−10	1998 Nov 18	15.90±0.08	0.08±0.18	0.38±0.22	2001 JU3	

^aAll objects are listed with their 2MASS ADR Point Source Catalog source designations, given as “2MASS Jhhmmss[.]ss±ddmmss[.]s”. The suffix is the sexagesimal Right Ascension and declination at J2000 equinox.

^bPhotometry from the 2MASS ADR; note that some objects have revised photometry placing them outside of our original WPSD search constraints.

^cAsteroid identifications are from the Small-Body Search Tool maintained by the Jet Propulsion Laboratory Solar System Dynamics Group: http://ssd.jpl.nasa.gov/cgi-bin/sb_search.

TABLE 2
LOG OF SPEX PRISM OBSERVATIONS: T DWARF CANDIDATES.

Object (1)	J^a (2)	$J - H^a$ (3)	$H - K_s^a$ (4)	UT Date (5)	t (s) (6)	Airmass (7)	Calibrator (8)	SpT (9)	Identification ^b (10)
2MASS J00013044+1010146	15.83±0.07	0.69±0.12	-0.07±0.07	2003 Sep 19	720	1.02	HD 210501	A0 V	M6V
2MASS J00115060-1523450	15.93±0.08	0.29±0.17	0.38±0.08	2003 Sep 18	720	1.29	HD 219833	A0 V	M7.5Ve
2MASS J00335534-0908247	15.96±0.09	0.96±0.14	-0.24±0.09	2003 Sep 19	720	1.15	HD 1154	A0 V	M8Ve:
2MASS J00345157+0523050	15.54±0.05	0.09±0.09	< -0.8	2003 Sep 05	1800	1.05	HD 5267	A1 Vn	T7
2MASS J00412179+3547133	15.94±0.08	0.21±0.17	0.56±0.08	2003 Sep 19	720	1.08	HD 13869	A0 V	sdL?
2MASS J00552554+4130184	15.81±0.08	0.84±0.11	-0.02±0.08	2003 Sep 18	720	1.16	HD 7215	A0 V	M8Ve:
2MASS J00583814-1747311	15.94±0.09	0.20±0.19	0.27±0.09	2003 Sep 18	720	1.28	HD 219833	A0 V	M6V
2MASS J01045111-3327380	15.96±0.10	0.19±0.19	0.94±0.10	2003 Sep 18	720	1.72	HD 12275	A0 V	M8V
2MASS J01151621+3130061	15.89±0.10	0.22±0.20	0.66±0.24	2003 Sep 19	720	1.05	HD 13869	A0 V	M8.5Ve
2MASS J01423153+0523285	15.91±0.08	0.32±0.14	-0.01±0.08	2003 Sep 17	720	1.05	HD 18571	A0 V	sdM7.5?
2MASS J01470204+2120242	15.99±0.07	0.97±0.21	-0.01±0.07	2003 Sep 18	720	1.09	HD 7215	A0 V	M7.5Ve:
2MASS J01532750+3631482	15.81±0.06	0.66±0.11	0.44±0.06	2003 Sep 18	720	1.10	HD 7215	A0 V	M6V
2MASS J03023398-1028223	16.24±0.12	0.52±0.19	0.60±0.12	2003 Sep 17	720	1.17	HD 25792	A0 V	M5.5V
2MASS J04035944+1520502	15.97±0.08	0.29±0.16	0.42±0.08	2003 Sep 19	720	1.03	HD 25175	A0 V	M7V
2MASS J04070885+1514565	16.06±0.09	0.04±0.23	0.10±0.09	2003 Sep 19	1080	1.01	HD 25175	A0 V	T5.5
2MASS J04071296+1710474	16.01±0.10	0.32±0.19	0.54±0.10	2003 Sep 19	720	1.00	HD 25175	A0 V	M8V
2MASS J04360273+1547536	16.13±0.09	0.98±0.12	0.22±0.09	2003 Sep 18	720	1.00	HD 25175	A0 V	M6.5V
2MASS J11070582+2827226	15.74±0.06	0.57±0.12	0.11±0.06	2003 May 23	1080	1.01	HD 89239	A0 V	M8Ve
2MASS J11150577+2520467	15.85±0.08	0.82±0.11	-0.04±0.08	2003 May 23	1080	1.01	HD 89239	A0 V	M7.5Ve:
2MASS J11323833-1446374	15.83±0.09	0.20±0.14	0.29±0.09	2003 May 21	1200	1.00	HD 101369	A0 V	M7V
2MASS J11463232+0203414	15.89±0.09	0.21±0.19	0.21±0.09	2003 May 22	1200	1.05	HD 97585	A0 V	M5.5V
2MASS J12095613-1004008	15.91±0.07	0.58±0.12	0.27±0.07	2003 May 22	1440	1.02	HD 109309	A0 V	T3
				2003 May 23	1080	1.16	HD 109309	A0 V	
2MASS J12121714-2253451	15.69±0.07	0.28±0.16	0.37±0.07	2003 May 23	720	1.39	HD 110649	A0 V	M8Ve
2MASS J12314753+0847331	15.57±0.07	0.26±0.13	0.09±0.07	2003 May 21	1080	1.02	HD 111744	A0 V	T6
2MASS J12575768-0204085	15.71±0.17	0.46±0.25	0.48±0.17	2003 May 22	1080	1.11	HD 109309	A0 V	sd:M5
2MASS J13272391+0946446	15.99±0.10	0.65±0.15	-0.06±0.10	2003 May 23	720	1.02	HD 116960	A0 V	M6V
2MASS J13593574+3031039	15.87±0.08	0.26±0.14	0.34±0.08	2003 May 21	800	1.05	HD 121626	A0	M7V
2MASS J14171672-0407311	15.95±0.07	0.59±0.10	-0.12±0.07	2003 May 22	1080	1.10	HD 126129	A0 V	M8Ve:
2MASS J15243203+0934386	15.05±0.05	0.79±0.08	-0.04±0.05	2003 May 22	720	1.04	HD 136831	A0 V	M7Ve:
2MASS J15412408+5425598	15.93±0.08	0.26±0.18	0.32±0.08	2003 May 21	1080	1.22	HD 142282	A0	M8Ve
2MASS J15561873+1300527	15.91±0.07	0.13±0.17	0.93±0.07	2003 May 23	720	1.01	HD 140729	A0 V	M8.5Ve
2MASS J15590462-0356280	15.97±0.07	0.25±0.17	< 0.3	2003 May 21	720	1.10	HD 143396	A0	M8.5Ve
2MASS J16304206-0232224	15.49±0.06	0.51±0.10	0.23±0.06	2003 May 22	720	1.09	HD 145647	A0 V	M8V
2MASS J16390818+2839015	15.85±0.08	0.50±0.13	0.48±0.08	2003 May 23	720	1.02	HD 145647	A0 V	M7.5V

TABLE 2—Continued

Object (1)	J^a (2)	$J - H^a$ (3)	$H - K_s^a$ (4)	UT Date (5)	t (s) (6)	Airmass (7)	Calibrator (8)	SpT (9)	Identification ^b (10)
2MASS J16403197+1231068	15.95±0.08	0.34±0.14	< 0.4	2003 May 21	720	1.01	HD 151545	A0	sdM8?
2MASS J16403561+2922225	15.70±0.07	0.63±0.10	0.40±0.07	2003 May 22	720	1.07	HD 145647	A0 V	sdM8?
2MASS J17252029-0024508	15.91±0.08	0.87±0.11	-0.03±0.08	2003 May 23	720	1.14	HD 171149	A0 V	M5V
2MASS J17330480+0041270	15.91±0.10	0.13±0.19	0.37±0.10	2003 May 21	720	1.06	HD 159835	A0	M7V
2MASS J17331764+1529116	15.91±0.07	0.45±0.14	< 0.0	2003 May 21	720	1.01	HD 159907	A0	DC 10
2MASS J17364839+0220426	15.85±0.08	0.49±0.13	0.47±0.08	2003 May 23	720	1.13	HD 171149	A0 V	M8V
2MASS J18112466+3748513	15.54±0.05	0.32±0.08	-0.26±0.05	2003 May 22	720	1.07	HD 174567	A0 V	mid M::
2MASS J18244344+2937133	15.89±0.08	0.08±0.15	< 0.1	2003 May 23	720	1.08	HD 165029	A0 V	M6V
2MASS J18283572-4849046	15.18±0.06	0.27±0.09	-0.27±0.06	2003 Sep 18	1080	2.7-2.8	HD 177406	A0 V	T6
2MASS J18411320-4000124	15.94±0.06	0.92±0.11	-0.20±0.06	2003 Sep 17	720	2.07	HD 176425	A0 V	M7.5Ve:
2MASS J18530004-4133275	15.68±0.07	0.62±0.11	-0.05±0.07	2003 Sep 18	720	2.10	HD 176425	A0 V	M7 pec
2MASS J19010601+4718136	15.86±0.07	0.39±0.12	-0.17±0.07	2003 May 21	1440	1.13	HD 177390	A0	T5
2MASS J19240765-2239504	15.97±0.09	0.24±0.17	0.40±0.09	2003 May 21	1080	1.37	HD 174072	A0 V	M6V
2MASS J19312708+5948588	15.47±0.07	0.59±0.11	0.20±0.07	2003 Sep 18	720	1.35	HD 194354	A0 Vs	M5.5V
2MASS J19445221-0831036	15.82±0.06	0.50±0.10	-0.08±0.06	2003 Sep 17	720	1.18	HD 188489	A0 V	M6V
2MASS J19522109-5059169	15.96±0.08	0.30±0.19	0.76±0.08	2003 Sep 18	720	3.04	HD 183626	A0 V	M6V
2MASS J19570817-1627558	15.84±0.09	0.29±0.17	0.77±0.09	2003 Sep 19	720	1.32	HD 198787	A0 V	M6V
2MASS J20494090+1140068	16.26±0.10	0.62±0.18	0.69±0.10	2003 Sep 17	720	1.02	HD 210501	A0 V	M7.5V
2MASS J21100889+2132483	15.94±0.08	0.66±0.11	0.000±0.08	2003 Sep 17	720	1.01	HD 210501	A0 V	M8V
2MASS J21105305+1903568	15.94±0.08	0.17±0.14	0.71±0.08	2003 Sep 19	720	1.02	HD 210501	A0 V	M8.5Ve
2MASS J21214516+2825375	15.81±0.08	0.28±0.15	0.74±0.08	2003 Sep 19	720	1.06	HD 210501	A0 V	M7.5V
2MASS J21353463+2352085	16.10±0.12	0.67±0.16	0.05±0.12	2003 Sep 19	720	1.06	HD 210501	A0 V	M7V
2MASS J22270083-1231482	15.68±0.06	0.49±0.10	-0.13±0.06	2003 Sep 17	720	1.18	HD 219833	A0 V	M5.5V
2MASS J22425680+0720249	16.05±0.10	0.88±0.15	0.14±0.10	2003 Sep 18	720	1.03	HD 210501	A0 V	M8Ve:
2MASS J22453832-0722060	16.11±0.09	0.55±0.14	0.18±0.09	2003 Sep 17	720	1.12	HD 219833	A0	M7 pec
2MASS J22465014-0643357	15.50±0.06	0.53±0.11	0.29±0.06	2003 Sep 17	720	1.12	HD 219833	A0	M5V
2MASS J23270985+2341364	15.99±0.10	0.24±0.19	0.35±0.10	2003 Sep 17	720	1.10	HD 222749	A0 V	M7.5Ve:
2MASS J23312378-4718274	15.66±0.07	0.15±0.16	0.12±0.07	2003 Sep 17	720	2.7-2.8	HD 216009	A0 V	T5
2MASS J23354680+1257273	15.83±0.06	0.12±0.15	0.70±0.06	2003 Sep 18	720	1.02	HD 210501	A0 V	M8.5Ve
2MASS J23363834+4523306	15.99±0.10	0.61±0.15	-0.27±0.10	2003 Sep 17	720	1.26	HD 222749	A0 V	M8V
2MASS J23480816+4052343	16.11±0.09	0.46±0.16	0.54±0.09	2003 Sep 17	720	1.23	HD 222749	A0 V	M7.5V
2MASS J23592315-1239079	15.96±0.07	0.28±0.15	0.72±0.07	2003 Sep 18	720	1.22	HD 219833	A0 V	M7V

^aPhotometry from the 2MASS ADR; note that some objects have revised photometry outside of our original WPSD search constraints.

^bClassifications are based on comparison to spectral templates (Table 3) and for M dwarfs are accurate to within 0.5-1.0 subclasses (see § 3.1.1). Classification terms followed by a colon (":") are more uncertain due to poor S/N data or lack of adequate comparison stars.

TABLE 3
LOG OF SPEX PRISM OBSERVATIONS: COMPARISON STARS.

Object (1)	<i>J</i> ^a (2)	<i>J</i> − <i>H</i> ^a (3)	<i>H</i> − <i>K_s</i> ^a (4)	UT Date (5)	t (s) (6)	Airmass (7)	Calibrator (8)	SpT (9)	Identification (10)	Ref (11)
2MASS J01514155+1244300	16.57±0.13	0.96±0.17	0.42±0.13	2003 Sep 19	1080	1.03	HD 13869	A0 V	T1:	1
2MASS J02431371−2453298	15.38±0.05	0.24±0.12	−0.08±0.05	2003 Sep 17	1080	1.42	HD 27616	A0 V	T6	2
2MASS J04151954−0935066	15.70±0.06	0.16±0.13	0.11±0.06	2003 Sep 17	1080	1.15	HD 25792	A0 V	T8	2
2MASS J04234858−0414035	14.47±0.03	1.00±0.04	0.53±0.03	2003 Sep 17	720	1.10	HD 31411	A0 V	T0	1
2MASS J11040127+1959217	14.38±0.03	0.90±0.04	0.53±0.03	2003 May 21	960	1.02	HD 101060	A0 V	L4	3
2MASS J11240487+3808054	12.71±0.02	0.70±0.04	0.45±0.02	2003 May 22	360	1.05	HD 98152	A0 V	M8.5V	3
2MASS J12255432−2739466AB	15.26±0.05	0.16±0.09	0.02±0.05	2003 May 23	720	1.55	HD 110141	A0 V	T6/T8:	4,5
2MASS J12545393−0122474	14.89±0.04	0.80±0.04	0.25±0.04	2003 May 22	720	1.08	HD 109309	A0 V	T2	6
2MASS J14392836+1929149	12.76±0.02	0.72±0.03	0.50±0.02	2003 May 23	360	1.00	HD 122945	A0 V	L1	7
2MASS J14571496−2121477	15.32±0.05	0.06±0.10	0.03±0.05	2003 May 22	1080	1.33	HD 133466	A0 V	Gl 570D, T8	8
2MASS J15031961+2525196	13.94±0.02	0.08±0.04	−0.11±0.02	2003 May 22	720	1.02	HD 136831	A0 V	T5.5	9
2MASS J15261405+2043414	15.59±0.06	1.09±0.07	0.57±0.06	2003 May 23	720	1.05	HD 140729	A0	L7	10
2MASS J16241436+0029158	15.49±0.05	−0.03±0.11	< 0.0	2003 May 22	1440	1.09	HD 145647	A0 V	T6	11
2MASS J16322911+1904407	15.87±0.07	1.25±0.08	0.61±0.07	2003 May 22	1080	1.07	HD 145647	A0 V	L8	7
2MASS J17072343−0558249AB	12.05±0.02	0.79±0.04	0.55±0.02	2003 May 23	960	1.19	HD 171149	A0 V	M9V/L3	12,13
2MASS J17361766+1346225	10.41±0.02	0.60±0.03	0.28±0.02	2003 May 21	180	1.05	HD 165029	A0 V	LP 508-14, M4V	14
2MASS J17503293+1759042	16.34±0.10	0.39±0.17	0.47±0.10	2003 May 23	1080	1.08	HD 165029	A0 V	T3.5	1
2MASS J18261131+3014201	11.66±0.02	0.48±0.03	0.36±0.02	2003 May 21	240	1.18	HD 174567	A0 Vs	M8.5V	15
2MASS J19165762+0509021	9.91±0.03	0.68±0.04	0.46±0.03	2003 Sep 19	200	1.04	HD 189920	A0 V	VB10, M8V	16
2MASS J20282035+0052265	14.30±0.04	0.92±0.05	0.58±0.04	2003 May 23	720	1.06	HD 198070	A0 Vn	L3	17
2MASS J20362186+5059503	13.61±0.03	0.45±0.05	0.22±0.05	2003 Sep 18	720	1.18	HD 194354	A0 Vs	LSR 2036+50; sdM7.5	15,18
2MASS J20392378−2926335	11.36±0.03	0.61±0.03	0.38±0.03	2003 May 22	720	1.57	HD 202941	A0 V	M6V	19
2MASS J20491972−1944324	12.85±0.02	0.63±0.03	0.44±0.02	2003 Sep 19	360	1.34	HD 198787	A0 V	M7.5V	19
2MASS J20575409−0252302	13.12±0.02	0.85±0.03	0.54±0.02	2003 May 23	360	1.09	HD 198070	A0 Vn	L1.5	20
2MASS J21073169−0307337	14.20±0.03	0.76±0.04	0.56±0.03	2003 May 23	720	1.10	HD 198070	A0 Vn	M9V	3, 21
2MASS J21225635+3656002	13.71±0.03	0.41±0.05	0.18±0.05	2003 Sep 18	720	1.05	HD 209932	A0 V	LSR 2122+36; esdM5	15,18
2MASS J22120345+1641093	11.43±0.03	0.60±0.04	0.28±0.03	2003 Sep 19	240	1.03	HD 210501	A0 V	M5V	14
2MASS J22282889−4310262	15.66±0.07	0.30±0.14	0.07±0.07	2003 Sep 17	1080	2.3−2.4	HD 216009	A0 V	T6.5	22
2MASS J22341394+2359559	13.15±0.02	0.79±0.03	0.52±0.03	2003 Sep 19	360	1.02	HD 210501	A0 V	M9.5V	19
2MASS J22541892+3123498	15.26±0.05	0.24±0.09	0.12±0.05	2003 Sep 18	720	1.04	HD 209932	A0 V	T4	2
V* V1451 Aql	2.3±0.3	0.9±0.4	0.3±0.4	2003 May 22	12	1.16	HD 185533	A0 V	M5IIb	23
V* Z Cep	5.95±0.03	0.88±0.05	0.67±0.05	2003 May 22	72	1.27	HD 203893	A0 V	MIab ^b	23
SV* P 2312	1.9±0.3	0.9±0.4	0.4±0.4	2003 May 22	12	1.28	HD 203893	A0 V	M7IIIb	23

^aPhotometry from the 2MASS ADR.

^bSpectral types for variable giant stars may vary by several subclasses over time, and given classifications may not accurately represent the actual spectrum observed.

References. — (1) Geballe et al. (2002); (2) Burgasser et al. (2002); (3) Cruz et al. (2003); (4) Burgasser et al. (1999); (5) Burgasser et al. (2003e); (6) Leggett et al. (2000); (7) Kirkpatrick et al. (1999); (8) Burgasser et al. (2000); (9) Paper I; (10) Kirkpatrick et al. (2000); (11) Strauss et al. (1999); (12) Gizis (2002); (13) McElwain & Burgasser, in prep.; (14) J. Gizis, priv. comm.; (15) Lepine, Shara, & Rich (2002); (16) Kirkpatrick, Henry, & McCarthy (1991); (17) Hawley et al. (2002); (18) Lepine, Rich, & Shara (2003a); (19) Gizis et al. (2000); (20) Kirkpatrick & Tinney, in prep.; (21) Cruz et al., in prep.; (22) Paper II; (23) SIMBAD

TABLE 4
LOG OF SPEX SXD OBSERVATIONS.

Object (1)	SpT (2)	UT Date (3)	t (s) (4)	Airmass (5)	Calibrator (6)	SpT (7)
2MASS J00345157+0523050	T7	2003 Sep 19	3000	1.04	HD 6457	A0 Vn
2MASS J12314753+0847331	T6	2003 May 21	3000	1.08	HD 111744	A0 V
2MASS J15031961+2525196	T5.5	2003 May 23	1800	1.01	HD 131951	A0 V
2MASS J18283572-4849046	T6	2003 Sep 19	3000	2.7-2.8	HD 177406	A0 V
2MASS J19010601+4718136	T5	2003 Sep 19	2400	1.19	HD 178207	A0 Vn
2MASS J23312378-4718274	T5	2003 Sep 18	2400	2.5-2.6	HD 216009	A0 V

TABLE 5
SPECTRAL AND PHOTOMETRIC PROPERTIES OF 2MASS T DWARF DISCOVERIES.

Name (1)	SpT (2)	2MASS <i>J</i> (3)	<i>J</i> - <i>H</i> (4)	<i>H</i> - <i>K_s</i> (5)	<i>d</i> ^a (pc) (6)
2MASS 0034+0523	T7	15.54±0.05	0.09±0.09	< -0.8	8.2±1.4
2MASS 0407+1514	T5.5	16.06±0.09	0.04±0.23	0.10±0.33	19±3
2MASS 1209-1004	T3	15.91±0.07	0.58±0.12	0.27±0.17	23.2±2.1
2MASS 1231+0847	T6	15.57±0.07	0.26±0.13	0.09±0.22	12.0±2.4
2MASS 1828-4849	T6	15.18±0.06	0.27±0.09	-0.27±0.16	10.6±2.1
2MASS 1901+4718	T5	15.86±0.07	0.39±0.12	-0.17±0.30	20±3
2MASS 2331-4718	T5	15.66±0.07	0.15±0.16	0.12±0.25	18.0±2.5

^aSpectrophotometric distance estimate; see § 4.1.

TABLE 6
CLASSIFICATION INDICES FOR OBSERVED T DWARFS.

Name (1)	Prior	Indices ^a					Derived
	SpT ^b (2)	H ₂ O ^J (3)	CH ₄ ^J (4)	H ₂ O ^H (5)	CH ₄ ^H (6)	CH ₄ ^K (7)	SpT (8)
Standards							
SDSS 0423–0414	T0	0.62	0.95	0.64	1.07	0.83	
SDSS 1254–0122	T2	0.46	0.91	0.48	1.00	0.59	
2MASS 2254+3123	T4	0.36	0.87	0.39	0.63	0.31	
2MASS 0243–2453	T6	0.14	0.66	0.30	0.36	0.16	
2MASS 0415–0935	T8	0.04	0.44	0.18	0.11	0.05	
Known T Dwarfs							
SDSS 0151+1244	T1±1	0.64(0)	0.95(0)	0.64(0)	1.03(1)	0.70(1)	T0.5
SDSS 1750+1759	T3.5	0.46(2)	0.87(4)	0.45(3)	0.71(4)	0.35(4)	T3.5
2MASS 1503+2525	T5.5	0.24(5)	0.74(5)	0.34(5)	0.42(6)	0.20(5)	T5
2MASS 1225–2739AB	T6	0.17(6)	0.67(6)	0.28(6)	0.35(6)	0.18(6)	T6
SDSS 1624+0029	T6	0.16(6)	0.71(6)	0.31(6)	0.34(6)	0.14(6)	T6
2MASS 2228–4310	T6.5	0.15(6)	0.68(6)	0.29(6)	0.28(7)	0.12(7)	T6.5
Gliese 570D	T8	0.06(8)	0.50(8)	0.20(8)	0.15(8)	0.10(8)	T8
Discoveries							
2MASS 1209–1004		0.40(3)	0.83(4)	0.45(3)	0.77(3)	0.64(3)	T3
2MASS 1901+4718		0.28(5)	0.78(5)	0.36(5)	0.47(5)	0.24(5)	T5
2MASS 2331–4718		0.19(6)	0.72(5)	0.33(5)	0.49(5)	0.21(5)	T5
2MASS 0407+1514		0.23(5)	0.76(5)	0.34(5)	0.40(6)	0.16(6)	T5.5
2MASS 1828–4849		0.18(6)	0.70(6)	0.31(6)	0.40(6)	0.20(5)	T6
2MASS 1231+0847 ^c		0.18(6)	0.68(6)	0.27(6)	0.39(6)	0.17(6)	T6
2MASS 0034+0523		0.10(7)	0.64(6)	0.23(8)	0.25(7)	0.13(7)	T7

^aIndices are defined in Burgasser et al. (2003a). Values in parentheses for each index for known and new T dwarfs are the closest spectral type match to the standard indices; see Burgasser et al. (2002).

^bAssigned spectral types for spectral standards (Burgasser et al. 2002, 2003a); published spectral types for known T dwarfs (Burgasser et al. 2002; Geballe et al. 2002, objects in common have identical spectral types).

^cBased on combined spectral data over two nights.

TABLE 7
K I PSEUDO-EQUIVALENT WIDTHS.

Object (1)	SpT (2)	1.243 μm		1.252 μm	
		λ_c (μm) (3)	pEW (\AA) (4)	λ_c (μm) (5)	pEW (\AA) (6)
2MASS 1901+4718	T5	1.243	6.6 ± 0.8	1.252	8.9 ± 0.9
2MASS 2331-4718	T5	1.244	8.5 ± 0.7	1.252	12.8 ± 0.6
2MASS 1503+2525	T5.5	1.243	4.8 ± 0.3	1.252	7.4 ± 0.4
2MASS 1828-4849	T6	1.243	3.9 ± 0.7	1.252	6.6 ± 0.7
2MASS 1231+0847	T6	1.243	4.9 ± 0.6	1.253	6.7 ± 0.6
2MASS 0034+0523	T7	1.241	1.7 ± 0.5	1.252	3.9 ± 0.4

TABLE 8
KINEMATICS OF 2MASS T DWARF DISCOVERIES.

Name (1)	SpT (2)	μ ($'' \text{ yr}^{-1}$) (3)	θ ($^{\circ}$) (4)	V_{tan} (km s^{-1}) (5)	ΔT (yr) (6)	No. Stars Used in Fit (7)	Source ^a (8)
2MASS 0034+0523	T7	0.68 ± 0.06 0.70 ± 0.14	72 ± 4 74 ± 13	26 ± 5 27 ± 7	3.07 3.02	17 21	O A
2MASS 0407+1514	T5.5	< 0.09	...	< 8	5.19	13	O
2MASS 1209-1004	T3	0.46 ± 0.10	140 ± 8	51 ± 12	4.26	4	G
2MASS 1231+0847	T6	1.55 ± 0.07	228 ± 3	88 ± 18	3.24	20	A
2MASS 1828-4849	T6	0.33 ± 0.07	50 ± 12	17 ± 5	2.92	39	A
2MASS 1901+4718	T5	0.38 ± 0.02	197 ± 3	35 ± 6	5.27	62	O
2MASS 2331-4718	T5	< 0.10	...	< 9	2.90	13	A

^aO = Palomar 1.5m CCD *z*-band imaging; G = Lick 3.0m Gemini *J*-band imaging; A = AAT 3.9m IRIS2 CH₄-s imaging.

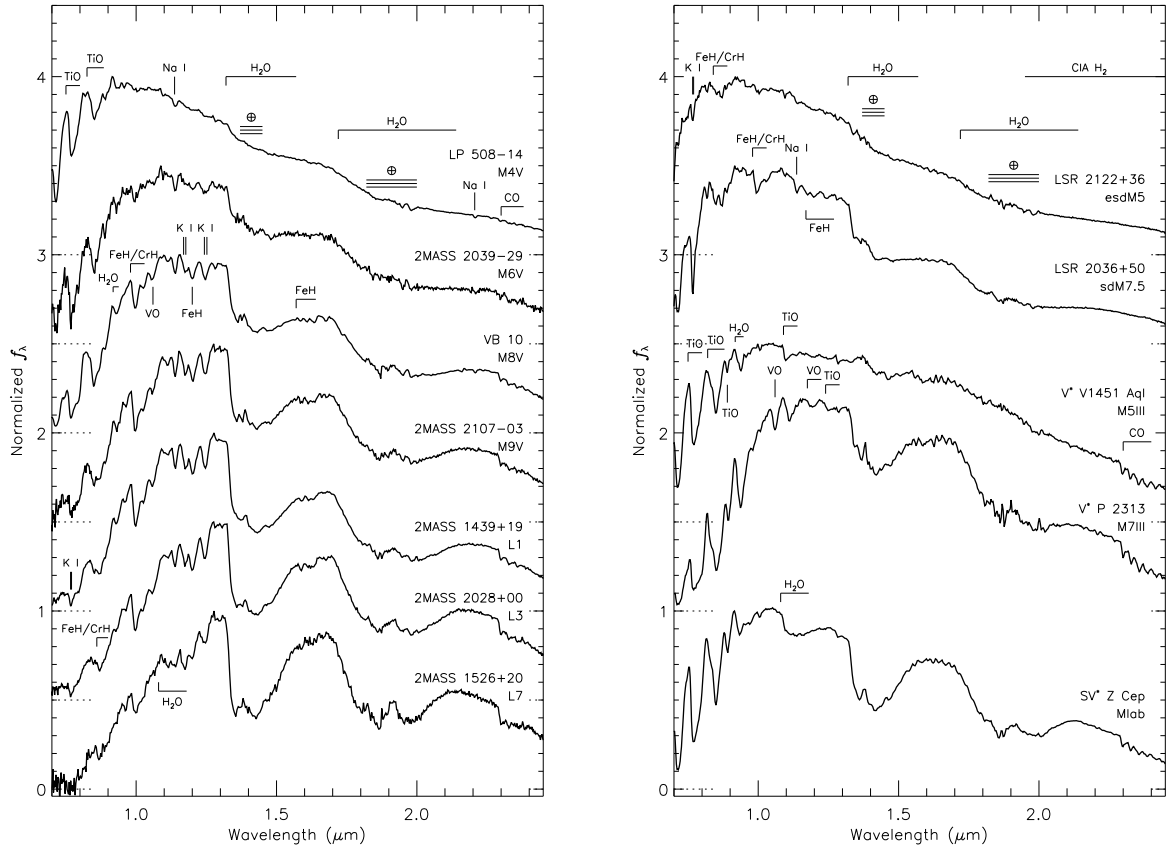


Fig. 1.— SpeX prism spectra for comparison stars. (Left) M and L dwarfs, including the optical spectral standards VB 10 (M8; Kirkpatrick, Henry, & McCarthy 1991) and 2MASS 1439+1929 (L1; Kirkpatrick et al. 1999). (Right) M-type subdwarfs, giants, and supergiants. Key spectral features are noted in both plots, as well as regions of strong telluric absorption (\oplus). All spectra are in units of F_λ normalized at their peak flux density and offset by a constant (dotted lines).

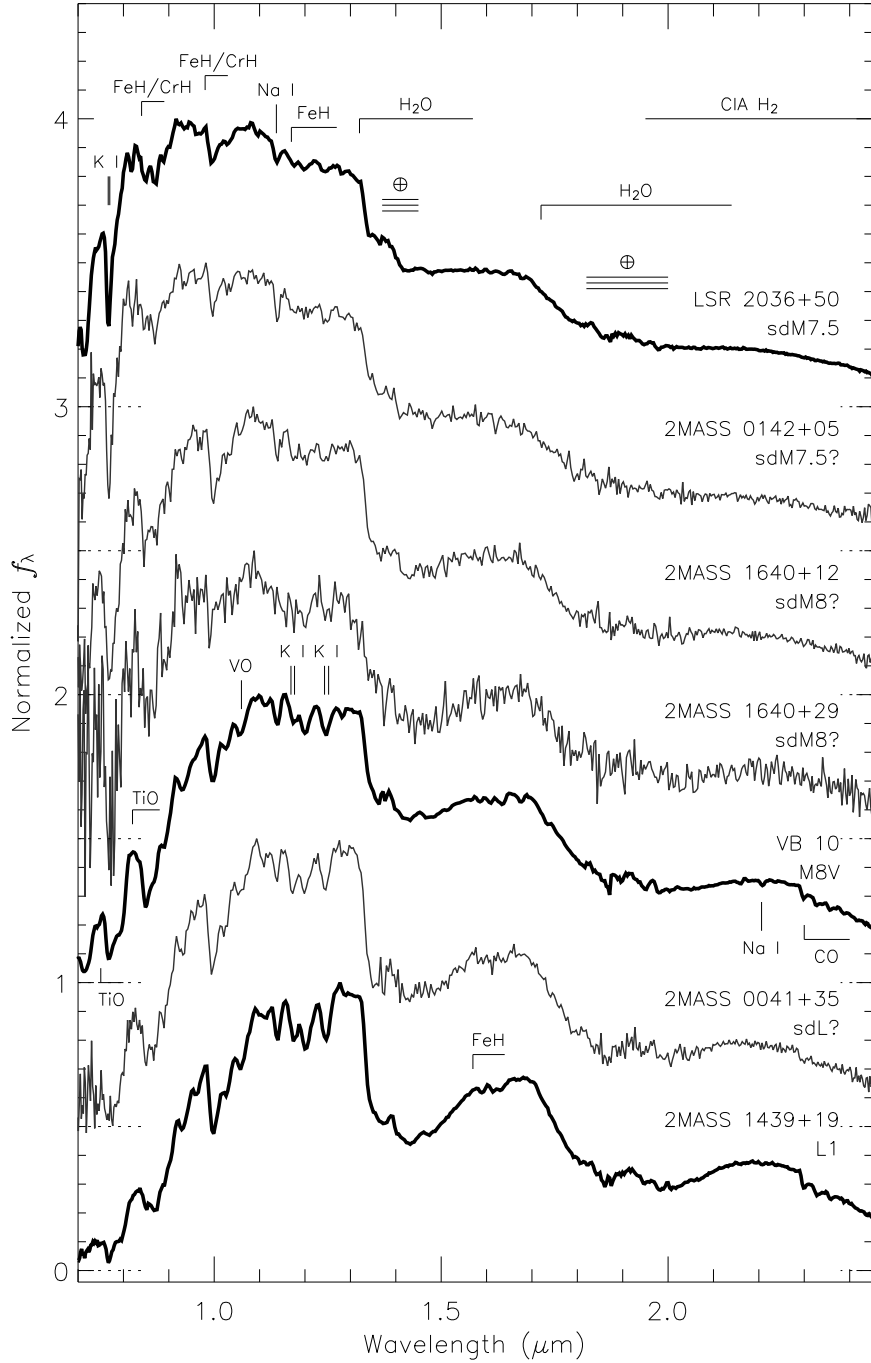


Fig. 2.— SpeX prism spectra of candidate subdwarfs (thin grey lines) identified in this sample. Spectra are normalized at their flux density peak and offset by a constant (dotted lines). Comparison stars LSR 2036+509 (sdM7.5), VB 10 (M8V), and 2MASS 1439+1929 (L1) are plotted with thick black lines. Features are noted as in Figure 1.

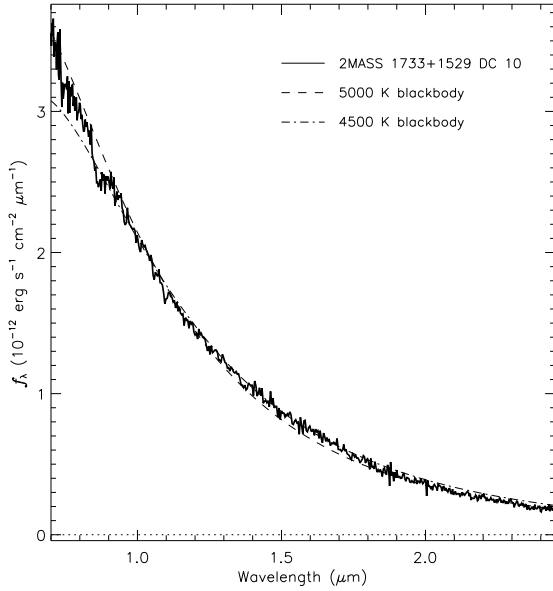


Fig. 3.— SpeX prism spectrum of 2MASS 1733+1529 (solid line). Best-fit blackbody curves of 5000 K (dashed line) and 4500 K (dot-dashed line) are shown.

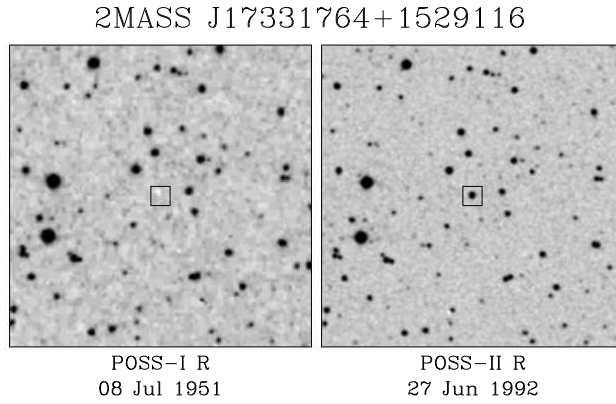


Fig. 4.— POSS-I (left) and POSS-II (right) R -band images of the 2MASS 1733+1529 field. Images are scaled to the same spatial resolution, 5' on a side, with North up and East to the left. The small proper motion measured for this object ($0.^{\circ}5 \pm 0.^{\circ}4 \text{ yr}^{-1}$) implies that its absence on the POSS-I R -band plate is not due to motion.

Fig. 5.— Finder charts for the T dwarf discoveries, showing second generation R -band DSS (POSS-II, SERC, AAO) and 2MASS (J - and K_s -bands) fields. Images are scaled and oriented as in Figure 4. [Note that these are now in gif format attached as separate files]

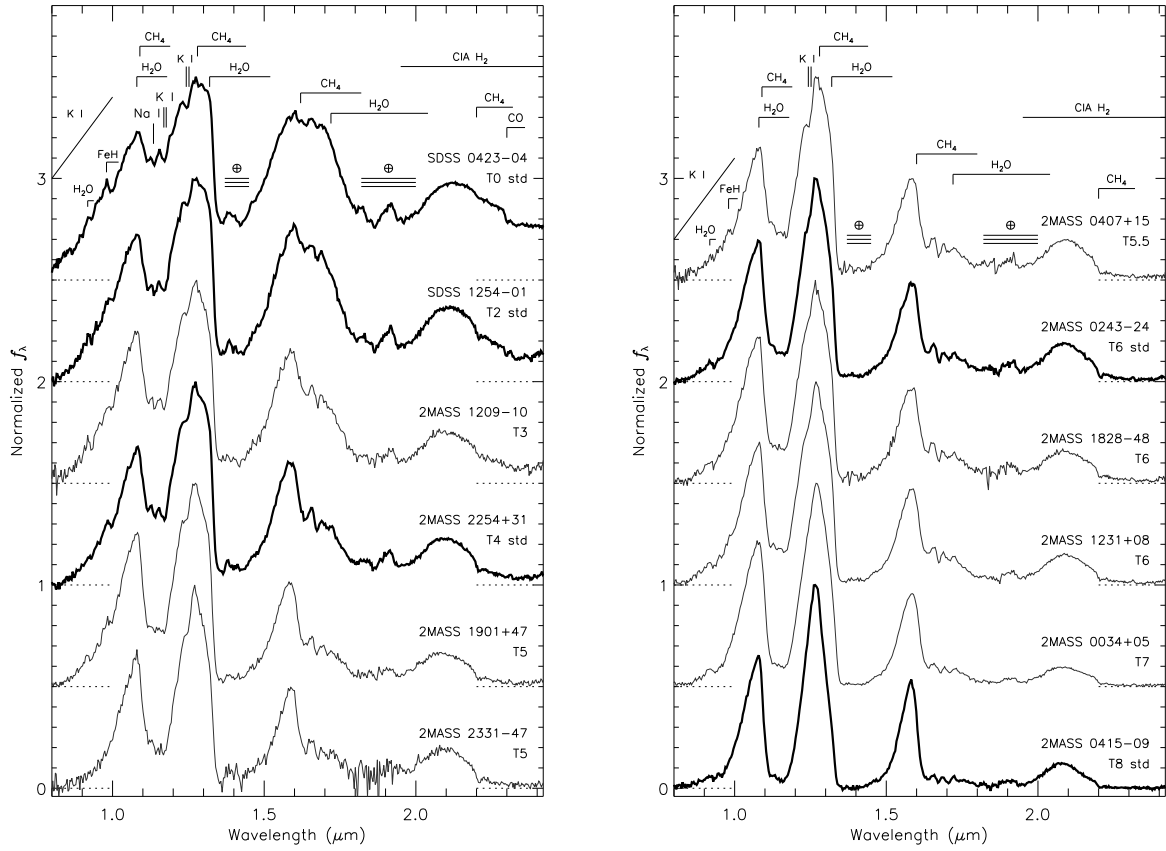


Fig. 6.— SpeX prism spectra of T dwarf discoveries (thin grey lines) and spectral standards (thick black lines). Spectra are normalized at $1.28 \mu\text{m}$ and offset by a constant (dotted lines). Key spectral features are indicated, as are regions of strong telluric absorption (\oplus).

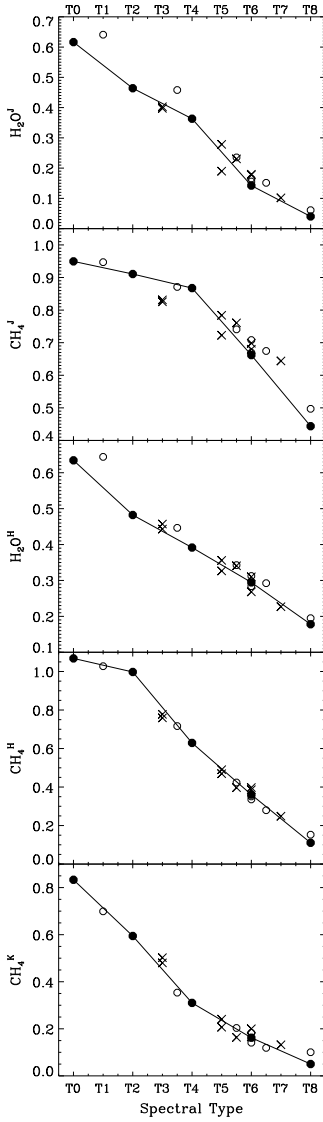


Fig. 7.— Spectral indices versus spectral type. Solid circles connected by lines indicate spectral standard values, open circles indicate previously known and classified T dwarfs, and crosses indicate T dwarf discoveries from this paper. Spectral types are those in Table 6, with assigned spectral types for the standards, previously published spectral types for the known T dwarfs, and derived spectral types for the new discoveries.

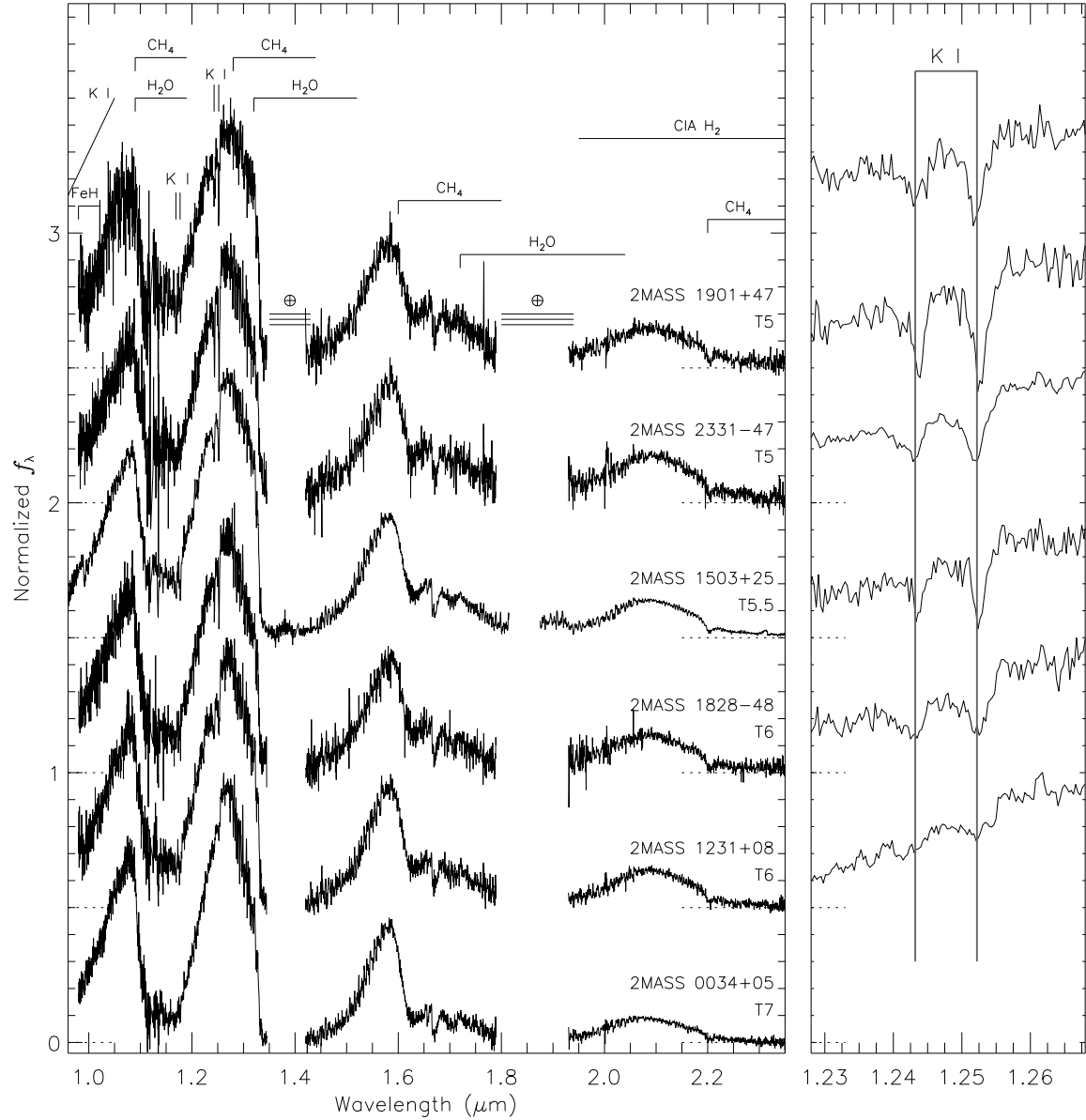


Fig. 8.— Moderate-resolution ($R \sim 1200$) SpeX spectra for six T dwarfs observed. (Left) Full spectra, normalized at $1.28 \mu\text{m}$ and offset by a constant (dotted lines). Regions of strong telluric absorption at 1.4 and $1.9 \mu\text{m}$ are omitted with the exception of the bright source 2MASS 1503+2525, where the gap between 1.79 and $1.84 \mu\text{m}$ is due to order separation. Features are noted as in Figure 7. (Right) Close-up of the spectral region around the $1.243/1.252 \mu\text{m}$ K I doublet. Spectra are scaled and offset as in the left panel.

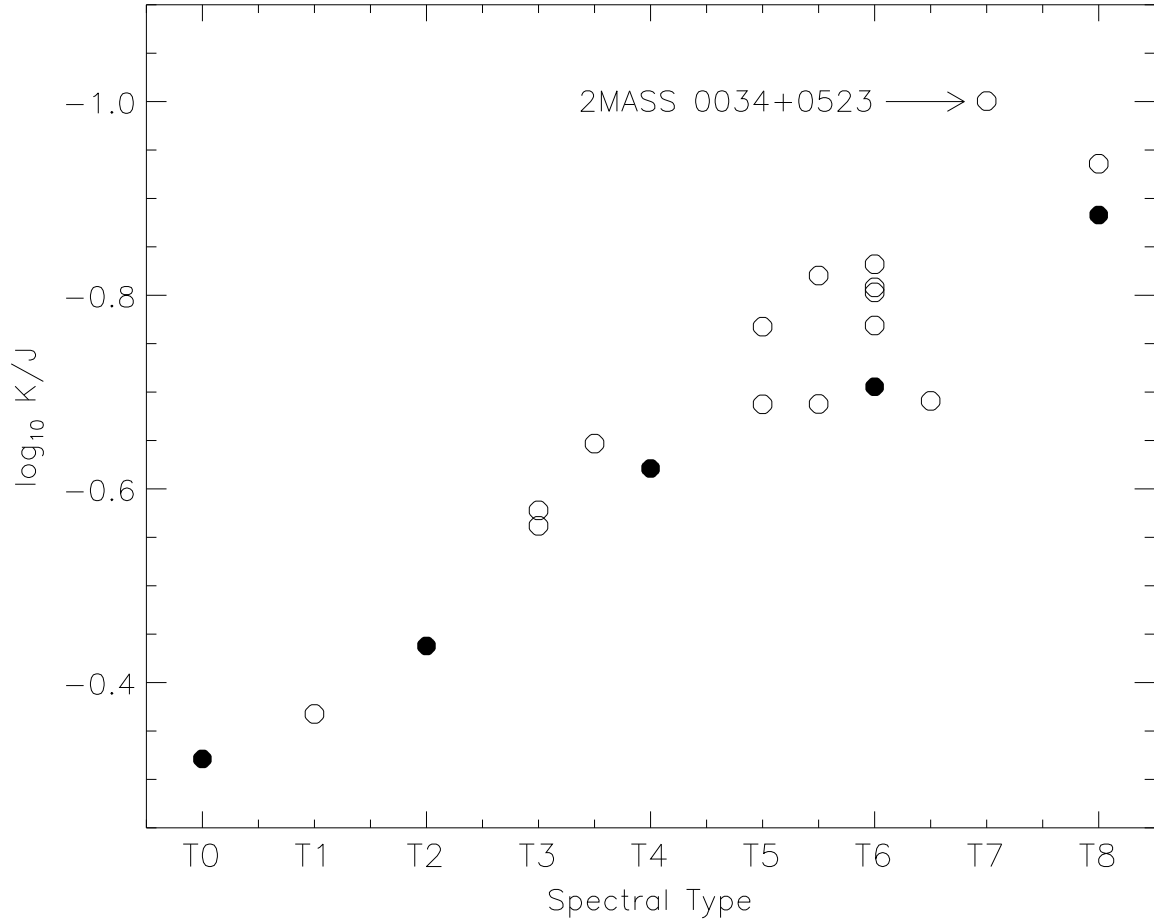


Fig. 9.— Spectral index $\log_{10} K/J$ versus T spectral type for objects observed with the SpeX low-resolution prism mode. Spectral standards are indicated by solid circles, all others are indicated by open circles. Note the excellent linear correlation across the full spectral type range, with the exception of 2MASS 0034+0523 (indicated) which exhibits a more suppressed K -band peak due to enhanced CIA H_2 absorption.

This figure "Burgasser.fig6a.jpg" is available in "jpg" format from:

<http://arxiv.org/ps/astro-ph/0402325v1>

This figure "Burgasser.fig6b.jpg" is available in "jpg" format from:

<http://arxiv.org/ps/astro-ph/0402325v1>

This figure "Burgasser.fig6c.jpg" is available in "jpg" format from:

<http://arxiv.org/ps/astro-ph/0402325v1>

This figure "Burgasser.fig6d.jpg" is available in "jpg" format from:

<http://arxiv.org/ps/astro-ph/0402325v1>

This figure "Burgasser.fig6e.jpg" is available in "jpg" format from:

<http://arxiv.org/ps/astro-ph/0402325v1>

This figure "Burgasser.fig6f.jpg" is available in "jpg" format from:

<http://arxiv.org/ps/astro-ph/0402325v1>

This figure "Burgasser.fig6g.jpg" is available in "jpg" format from:

<http://arxiv.org/ps/astro-ph/0402325v1>